

# FuXi-S2S: A skillful machine learning model for global subseasonal forecasts

Lei Chen<sup>1,2†</sup>, Xiaohui Zhong<sup>1,3†</sup>, Jie Wu<sup>4†</sup>, Deliang Chen<sup>5</sup>, Shangping Xie<sup>6</sup>, Qingchen Chao<sup>4</sup>, Chensen Lin<sup>3</sup>, Zixin Hu<sup>3</sup>, Bo Lu<sup>4\*</sup>, Hao Li<sup>1,3\*</sup> and Yuan Qi<sup>3,1\*</sup>

<sup>1</sup>Shanghai Academy of Artificial Intelligence for Science,  
Shanghai, 200232, China .

<sup>2</sup>INF, Shanghai, 200003, China .

<sup>3</sup>Artificial Intelligence Innovation and Incubation Institute,  
Fudan University, Shanghai, 200433, China.

<sup>4</sup>National Climate Center, China Meteorological Administration,  
Beijing, 100081, China.

<sup>5</sup>University of Gothenburg, Sweden.

<sup>6</sup>Scripps Institution of Oceanography, University of California  
San Diego, USA.

\*Corresponding author(s). E-mail(s): [bolu@cma.gov.cn](mailto:bolu@cma.gov.cn);  
[lihao\\_lh@fudan.edu.cn](mailto:lihao_lh@fudan.edu.cn); [qiyuan@fudan.edu.cn](mailto:qiyuan@fudan.edu.cn);

Contributing authors: [cltpys@163.com](mailto:cltpys@163.com); [x7zhong@gmail.com](mailto:x7zhong@gmail.com);  
[wujie@cma.gov.cn](mailto:wujie@cma.gov.cn); [deliang@gvc.gu.se](mailto:deliang@gvc.gu.se); [sxie@ucsd.edu](mailto:sxie@ucsd.edu);  
[chaoqc@cma.gov.cn](mailto:chaoqc@cma.gov.cn); [linchensen@fudan.edu.cn](mailto:linchensen@fudan.edu.cn);  
[huzixin@fudan.edu.cn](mailto:huzixin@fudan.edu.cn);

†These authors contributed equally to this work.

## Abstract

Subseasonal forecasts beyond 2 weeks pose a grand challenge for a wide range of applications across various sectors of society. Recently, machine learning based weather forecasting models have made remarkable advancements, outperforming the most successful numerical weather predictions (NWP) generated by the European Centre for Medium-Range Weather Forecasts (ECMWF). In this study, we introduce FuXi Subseasonal-to-Seasonal (FuXi-S2S), a machine learning based

subseasonal forecasting model that provides global daily mean forecasts for up to 42 days, covering 5 upper-air atmospheric variables at 13 pressure levels and 11 surface variables. FuXi-S2S integrates an enhanced FuXi base model with a perturbation module for flow-dependent perturbations in hidden features, and incorporates Perlin noise to perturb initial conditions. The model is developed using 72 years of daily statistics from ECMWF ERA5 reanalysis data. When compared to the ECMWF Subseasonal-to-Seasonal (S2S) reforecasts, the FuXi-S2S forecasts demonstrate superior deterministic and ensemble forecasts for total precipitation (TP), outgoing longwave radiation (OLR), and geopotential at 500 hPa (Z500). Moreover, it demonstrates comparable performance in predicting global 2-meter temperature (T2M), with clear advantages in land areas. Regarding forecasts for extreme TP, FuXi-S2S outperforms ECMWF S2S globally. Furthermore, FuXi-S2S surpasses the ECMWF S2S in predicting the Madden-Julian Oscillation (MJO), extending its skillful prediction from 30 days to 36 days. The MJO is a key source of subseasonal predictability and a significant driver of weather patterns around the world.

**Keywords:** subseasonal forecast, machine learning, deep learning, FuXi, MJO

## 1 Introduction

Subseasonal forecasting, is a method of predicting weather patterns that occur between 2 to 6 weeks or more in the future [1]. It is an important tool for various applications, such as agricultural planning, disaster preparedness and risk mitigation for extreme events like heatwaves, droughts, floods, and cold spells, as well as water resource management [2–5]. However, subseasonal forecasting is a challenging task due to its complex dependence on both local weather conditions and global climate system variables [6, 7]. Furthermore, the subseasonal time scale has long been considered as a ‘predictability desert’ [8, 9] as it suffers from the chaotic nature of the atmosphere [10] and the lack of predictive information from land beyond one month. Improving the representation of land-atmosphere coupling and predictions for the subseasonal Madden-Julian oscillation (MJO) in models is considered essential for bridging this predictability gap. Despite these challenges, skillful subseasonal forecasts are crucial for making informed decisions in various fields.

Subseasonal forecasts like their medium-range counterparts, mostly rely on conventional physics-based numerical weather prediction (NWP) models. However, in subseasonal forecasting, ensemble forecasts are essential as deterministic predictions lose all forecast skills compared to climatology [11]. The European Centre for Medium-Range Weather Forecasts (ECMWF) ensemble prediction system (EPS) [12] and the National Centers for Environmental Prediction (NCEP) Climate Forecast System version 2 (CFS v2) [13] are two leading operational subseasonal ensemble forecast systems, with 51 and 11

members, respectively. Nevertheless, these NWP forecasts exhibit considerable biases [7, 14], particularly in predicting extreme events [15].

To improve the accuracy of subseasonal forecasts, several competitions have been launched with a specific focus on subseasonal forecasts of 2-meter temperature (T2M) and total precipitation (TP). These include the United States (U.S.) Bureau of Reclamation (USBR) Sub-Seasonal Climate Forecasting Rodeos [16] and the World Meteorological Organization (WMO) Subseasonal-to-Seasonal (S2S) Artificial Intelligence (AI) Challenge [17]. The primary objective of these competitions is to apply machine learning models for postprocessing ensemble outputs from the state-of-the-art NWP models for forecast lead times of weeks 3-4 and weeks 5-6. While many top-performing models from participants demonstrated superior performance in subseasonal forecasts compared to physics-based operational subseasonal forecasts, these machine learning models still rely on forecasts from NWP models as inputs. Running NWP models requires substantial computational resources. A promising alternative is to develop machine learning models for direct subseasonal forecasting [18].

Machine learning models have the advantages of higher computational efficiency, facilitating the generation of large number of ensemble members which are crucial for prediction skill and forecast reliability [19]. Recent years have witnessed significant breakthroughs in the field of machine learning based weather forecasting, especially for temporal scales ranging from a few days to around 2 weeks, as demonstrated in multiple key studies [20–24]. These machine learning models have shown superior performance compared to the ECMWF high-resolution forecast (HRES), widely regarded as the most accurate global weather forecast model [25]. Despite notable progress has been made in machine learning based subseasonal forecasting model, challenges persist. For instance, Weyn et al. [11] generated a 320-member ensemble forecast for 6 weeks using 32 slightly different U-Net models combined with 10 perturbed initial conditions. However, their model was found to be less accurate than the ECMWF S2S ensemble at week 3 and exhibited marginally lower accuracy for lead times of 4 and 5-6 weeks, when verified against ERA5 reanalysis data [26]. The authors acknowledged a notable limitation of their model is the lack of TP forecasts. He et al. [27] showed that, using climate variables as input, models like XGBoost [28, 29], multitask Lasso [30, 31], and an Encoder (LSTM)-Decoder (FNN) [32], outperformed the climatological baselines in predicting T2M and TP over the contiguous U.S. for weeks 3 and 4. Kiefer et al. [33] implemented quantile regression forecasts (QRFs) and random forest classifiers [34] to predict mean wintertime T2M and the occurrence of cold wave days in central Europe, using ERA5 reanalysis data as input. Their evaluations demonstrated improved forecasts relative to a climatological benchmarks. Despite recent advancements, the feasibility of developing a comprehensive machine learning based model surpassing the state-of-the-art NWP models in global subseasonal forecasting has yet to be demonstrated.

In this work, we present FuXi Subseasonal-to-Seasonal (FuXi-S2S), a machine learning based subseasonal forecasting model that generates global daily mean forecasts for 42 days from initialization. It includes 5 upper-air atmospheric variables at 13 pressure levels and 11 surface variables. FuXi-S2S produces deterministic forecasts of the ensemble mean and ensemble forecasts that exhibit superior performance compared to the ECMWF S2S ensemble, which is widely acknowledged as the most skillful S2S modeling system [5, 35]. Unlike FuXi, which consists of a cascade of three models for 15-day weather forecasts, FuXi-S2S is developed on an enhanced FuXi base model featuring a perturbation module and incorporation of Perlin noise for ensemble forecast generation. Conventional ensemble forecasts typically incorporate perturbations in both initial conditions and model physics. However, constructing initial condition perturbations is a complex task, requiring careful considerations of multivariate interactions and dynamic balance to prevent rapid dissipation of ensemble spread in model simulations [36]. Our perturbation module is innovative, introducing perturbations to hidden features, generating flow-dependent and spatially variable perturbations. Furthermore, Perlin noise is used to introduce additional perturbations to initial conditions. For model development, we use a dataset consisting of 72 years of daily statistics derived from 1-hourly ECMWF ERA5 reanalysis data at a spatial resolution of  $1.5^\circ$ . Validation was conducted for average forecasts for week 3 (days 15-21), week 4 (days 22-28), week 5 (days 29-35), and week 6 (days 36-42), weeks 3-4, and weeks 5-6. We compared FuXi-S2S forecast against the ECMWF's S2S ensemble from model cycle C47r3. FuXi-S2S demonstrates superior forecast performance, especially in predicting extreme TP. FuXi-S2S not only exhibits superior overall performance compared to ECMWF S2S but also demonstrates remarkable performance in specific extreme cases, such as the 2022 Pakistan floods. FuXi-S2S has shown capability to predict extreme rainfall events approximately 4 weeks in advance.

The MJO is recognized as the primary mode of intraseasonal variability in the tropics, initially discovered by Roland Madden and Paul Julian in the 1970s [37, 38]. This phenomenon features planetary-scale circulation and anomalous deep precipitating convection along the equator. It forms in the western tropical Indian Ocean and propagates eastward to the Pacific Ocean at an average speed of  $5 \text{ ms}^{-1}$  over 30-90 days [39]. The MJO has a significant impact on global weather and climate, serving as a major source of predictability on subseasonal timescales due to its quasi-periodic nature [39-42]. Current state-of-the-art dynamical forecasts can predict the MJO up to 3-4 weeks in advance, yet this falls short of the theoretical potential predictability of approximately 6-7 weeks, limited by model imperfections [42-44]. In recent years, increasing efforts have focused on applying machine learning models to improve MJO forecasts, either by post-processing dynamical forecasts [45, 46] or through direct forecasting [47-49]. However, only improving MJO predictions with machine learning models does not automatically ensure improved forecasts of related phenomena, such as tropical cyclones and monsoons, which also depend on

the model’s background state. Therefore, advancements in forecast models remain crucial for enhancing subseasonal predictions. In this study, we utilize the real-time multivariate MJO (RMM) index [50], along with the commonly used metrics of bivariate correlation coefficient (COR), to assess MJO forecast skill. Our evaluation of the ensemble mean from ECMWF S2S and FuXi-S2S shows that FuXi-S2S extends prediction skill from 30 to 36 days, surpassing ECMWF S2S, which is regarded as the most skillful MJO forecast model [51].

With the FuXi-S2S model’s comprehensive predictive capability, this work establishes the foundations for future machine learning studies into other leading modes of subseasonal variability, such as the Boreal Summer Intraseasonal Oscillation (BSISO) [52], North Atlantic Oscillation (NAO) [53], and East Asia-Pacific (EAP) teleconnection [54–56].

## 2 Results

This study evaluates the performance of the 51-member FuXi-S2S forecasts by analyzing testing data between 2017 and 2021, compared with the 11-member ECMWF S2S reforecasts from model cycle C47r3. Additionally, the performance of FuXi-S2S forecasts for the 2022 Pakistan floods is evaluated and compared to the 51-member ECMWF S2S real-time forecasts. The evaluation included deterministic metrics of the ensemble mean, probabilistic metrics for ensemble members, prediction skills for MJO forecasts, and specific performance for extreme events, such as the 2022 Pakistan floods.

### 2.1 Deterministic forecast metrics comparison

This subsection compares the performance of ensemble mean forecasts from FuXi-S2S and ECMWF S2S based on deterministic metrics. Figure 1 presents the globally-averaged and latitude-weighted temporal anomaly correlation coefficient (TCC) for both FuXi-S2S and ECMWF S2S, considering 4 variables: TP, T2M, geopotential at 500 hPa (Z500), and outgoing longwave radiation (OLR), across forecast lead times of 3, 4, 5, 6, 3-4, and 5-6 weeks. The analysis is based on the averaged TCC computed from all testing data spanning the period from 2017 to 2021. The FuXi-S2S forecasts generally demonstrate higher TCC values than the ECMWF S2S reforecasts for TP and OLR at all lead times, while comparable TCC values for Z500 and T2M. Specifically, regarding Z500, the FuXi-S2S forecasts are superior to the ECMWF S2S reforecasts at lead times of 3, 4, 5, and 3-4 weeks, and have marginally inferior performance at lead times of 6 and 5-6 weeks.

Supplementary Figure ?? provides the spatial distributions of temporally-averaged TCC for both ECMWF S2S and FuXi-S2S, along with the differences in TCC between FuXi-S2S and ECMWF S2S for TP, T2M, Z500, and OLR forecasts at lead times of 3-4 and 5-6 weeks, respectively. The spatial distributions of TCC reveal considerably higher values over tropics, and greater values over oceans than over land. The TCC differences are described in red (positive values), blue (negative values), and white (zero values) patterns, suggesting

whether FuXi-S2S’s performance is superior, inferior, or equivalent to ECMWF S2S, respectively. Overall, FuXi-S2S demonstrates positive TCC differences for TP and OLR in most regions worldwide, consistent with the findings presented in Figure 1. Moreover, FuXi-S2S also outperforms ECMWF over large part of extra-tropical regions for both T2M and Z500.

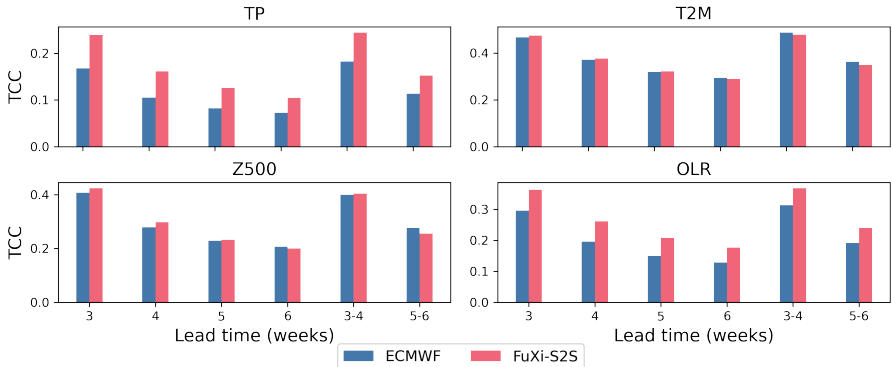


**Fig. 1:** Comparison of globally-averaged and latitude-weighted temporal anomaly correlation coefficient (TCC) of the ensemble mean between ECMWF S2S reforecasts (in blue) and FuXi-S2S forecasts (in red) for TP, T2M, Z500, and OLR. Rows 1 and 2 represent the performance across these variables, utilizing all testing data from the period spanning from 2017 to 2021.

## 2.2 Ensemble forecast metrics comparison

According to the comparative analysis of deterministic metrics, deterministic forecasts based on the ensemble mean exhibit limited skill, as shown by TCC values below 0.5 for all subseasonal forecast lead times. Therefore, ensemble forecasts are essential for detecting predictable signals at subseasonal timescales.

The first two rows of Figure 2 presents the spatial distribution of the temporally-averaged ranked probability skill score (RPSS)[57, 58] for ECMWF S2S and FuXi-S2S, as well as the RPSS differences between FuXi-S2S and ECMWF S2S for TP forecasts over 3-4 and 5-6 week lead times. This analysis utilizes RPSS data which are temporally averaged from 2017 to 2021. Global distributions of RPSS indicate that both ECMWF S2S and FuXi-S2S generally demonstrate considerably higher skills in tropical regions. Also, the RPSS values are considerably higher over oceans compared to land. The red contour lines in the first and second columns highlight areas with positive RPSS values, which indicate more skillful prediction than climatology forecast can be obtained over these areas. Notably, FuXi-S2S predicts more areas with positive RPSS values than ECMWF S2S. As in Figure ??, the color coding in

Figure 2 (red, blue, and white) indicates regions whether FuXi-S2S performs better, worse, or equivalently compared to ECMWF S2S, respectively. Predominantly, FuXi-S2S demonstrates nearly global positive RPSS differences for TP, except in some tropical regions where both models have quite high RPSS values. Compared to ECMWF S2S, whose skillful predictions primarily confined to tropical ocean areas, FuXi-S2S demonstrates the capability to provide skillful predictions over more extra-tropical regions, such as East Asia, the North Pacific and the Arctic.

The latitude-weighted RPSS for the same 4 variables as in Figure 1 over forecast lead times of 3, 4, 5, 6, 3-4, and 5-6 weeks are given in Supplementary Figure ???. Notably, FuXi-S2S shows consistently higher RPSS values than ECMWF S2S across all variables, namely TP, T2M, Z500, and OLR, especially over extratropical averages.

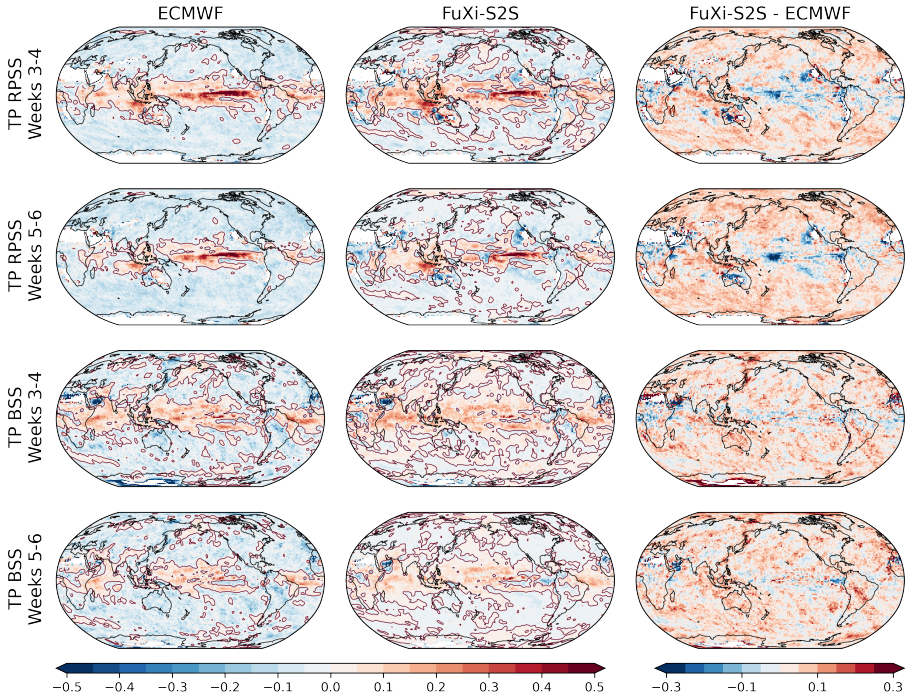


**Fig. 2:** Maps displaying the average Ranked Probability skill Score (RPSS) (first and second rows) and Brier Skill Score (BSS) (third and fourth rows) without latitude weighting, comparing ECMWF S2S (first column) and FuXi-S2S (second column) forecasts. Additionally, the third column depicts the difference in RPSS and BSS between FuXi-S2S and ECMWF S2S for TP at forecast lead times of weeks 3-4 (first and third rows) and weeks 5-6 (second and fourth rows), utilizing all testing data from 2017 to 2021. Red contour lines in the first and second columns indicate areas with positive values of RPSS and BSS.

### 2.3 Extreme forecast metrics comparison

One of the primary purposes of subseasonal forecasts lies in predicting extreme weather events, especially enhancing preparedness for disasters like droughts and floods. Therefore, this subsection focuses on analyzing the prediction skills for extreme precipitation events. Such events are identified when TP exceed the 90th climatological percentile, a threshold that varies based on grid location, forecast initialization time, and forecast lead time.

The last two rows of Figure 2 show the spatial distributions of the temporally-averaged Brier Skill Score (BSS)[58] for the extreme precipitation events, including BSS for ECMWF S2S and FuXi-S2S, and their differences over 3-4 and 5-6 week lead times. Similar to spatial pattern of RPSS, FuXi-S2S generally predicts more regions with positive values of BSS than ECMWF S2S, suggesting more areas with higher skills relative to climatological forecasts. Similar to spatial pattern of RPSS, the BSS values are considerably higher over oceans than land and decrease from lower latitudes to higher latitudes. Predominantly, the BSS differences favor FuXi-S2S in TP over land and in extra-tropical regions, marked by widespread red patterns. This suggests FuXi-S2S's dominance over ECMWF S2S in predicting extreme TP across land and extra-tropics, which is of great importance for disaster preparedness and mitigation of early warning.

Supplementary Figure ?? compares the latitude-weighted BSS between FuXi-S2S and ECMWF S2S, focusing on TP, T2M, Z500, and OLR in five geographical regions: global, in the extra-tropics ( $90^{\circ}\text{S} - 30^{\circ}\text{S}$  and  $30^{\circ}\text{N} - 90^{\circ}\text{N}$ ), in the tropics ( $30^{\circ}\text{S} - 30^{\circ}\text{N}$ ), over land, and over the ocean. Globally, FuXi-S2S outperforms ECMWF S2S in terms of BSS for TP, T2M, and OLR. Notably, in contrast to ECMWF S2S, which exhibits consistently negative globally-averaged BSS values for TP across all lead times, FuXi-S2S demonstrates positive values for forecast lead times of 3, 3-4 and 5-6 week. In the extra-tropical regions, though the BSS scores are relatively lower in comparison to the global average, FuXi-S2S consistently exhibits superior performance compared to ECMWF S2S across all four variables. A similar pattern emerges in tropical regions, where FuXi-S2S demonstrates superior performance over ECMWF S2S for TP and OLR, while achieving comparable accuracy in T2M and Z500. Over land areas, FuXi-S2S demonstrates consistently higher BSS values for TP and T2M, suggests its superior ability to provide more accurate forecasts of extreme rainfall and high temperatures compared to ECMWF S2S.

### 2.4 MJO forecast comparison

The RMM MJO index used for verification was calculated using the Climate Prediction Center (CPC) OLR (CBO) data, in conjunction with the ERA5 zonal-wind component at 850 hPa and 200h Pa. Figure 3 presents the bivariate correlation (COR) skills of RMM index for the ensemble mean of ECMWF S2S reforecasts and FuXi-S2S forecasts, averaged over the testing data spanning from 2017 to 2021. The results show a decrease in COR values as forecast

lead times increase. Particularly, FuXi-S2S outperforms ECMWF S2S in MJO prediction, maintaining higher COR values for up to 42 days. When applying a COR threshold of 0.5 to determine skillful MJO forecast, FuXi-S2S extends the skillful forecast lead time from 30 days to 36 days, surpassing the performance of ECMWF S2S. Furthermore, the MJO prediction skills also depend on the seasonal cycle, as illustrated in Figure 3. Both FuXi-S2S and ECMWF S2S demonstrate higher MJO prediction skills in September and October. Additionally, FuXi-S2S exhibit superior skills compared to ECMWF S2S during the boreal spring and winter, with skillful predictions extending beyond 42 days in April and May, which is the longest forecast lead time achievable by the FuXi-S2S model.

the skillful MJO prediction of FuXi-S2S exceeds 42 days, which is also the longest forecast lead time achievable by FuXi-S2S.

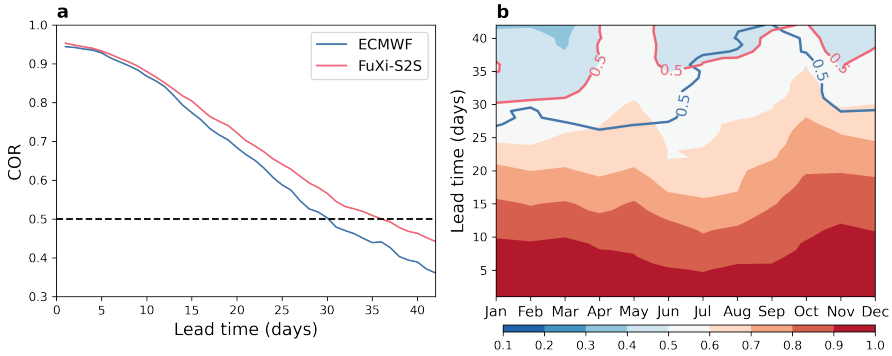


**Fig. 3:** Comparison of globally-averaged and latitude-weighted RMM bivariate Correlation (COR) (left column) of the ensemble mean between ECMWF S2S reforecasts (in blue) and FuXi-S2S forecasts (in red) using all testing data from 2017 to 2021. Dashed black line signifies the prediction skill threshold of  $COR=0.5$ . On the right column, the RMM bivariate COR is depicted as a function of the month of initialization (x-axis) and forecast lead time (y-axis), with red and blue lines indicating the skillful MJO prediction days of ECMWF S2S (in blue) and FuXi-S2S (in red), respectively.

A two-dimensional phase-space diagram is commonly used to characterize the phase and amplitude of the MJO, using the x-axis and y-axis to represent the first and second principal components of Empirical Orthogonal Functions (EOFs) (RMM1 and RMM2), respectively. Supplementary Figure ?? illustrates the forecast performance of four distinct MJO events with initialization dates of 27 June 2018, 3 November 2018, 18 April 2019, and 21 March 2021, as predicted by ECMWF S2S and FuXi-S2S. Data points on this two-dimensional phase-space diagram are plotted at 5-day intervals. The phase of the MJO is determined by the azimuth of the combined RMM indices 1 and 2 (RMM1 and

RMM2), while its amplitude is represented by the radial distance from the origin. As visually shown in the Supplementary Figure ??, the counterclockwise movement of data points signifies the eastward propagation of MJO-associated convection, with the distance between successive points reflecting the propagation speed. In comparison to the observed MJO derived from CBO and ERA5 reanalysis data, both ECMWF S2S and FuXi-S2S exhibit slower propagation speeds and reduced amplitudes as the forecast lead time increases, particularly noticeable for MJO forecasts initialized on 21 March 2021. However, FuXi-S2S shows a more consistent alignment with observations across all MJO phases, especially in mitigating the negative amplitudes biases in MJO forecasts when compared to ECMWF S2S.

## 2.5 2022 Pakistan floods

In 2022, Pakistan experienced a series of exceptionally intense monsoon rainfall surges from early July to late August, resulting in total rainfall that reached a level approximately four standard deviations above the climatological mean [59]. This extreme rainfall event led to a significant humanitarian disaster, leaving over 2.1 million people homeless and resulting in 1,730 fatalities. According to the World Bank, the economic damages and losses exceeded USD 30 billion [60]. Consequently, it is important to assess the ability of subseasonal forecasts to predict such extreme rainfall events.

Figure 4 illustrates the observed standardized TP anomaly alongside predictions that were initialized on different dates, generated by both the FuXi-S2S and ECMWF S2S models. These observations, taken from the Global Precipitation Climatology Project (GPCP), are spatially averaged over the Pakistan region (60 to 70°E in longitude and 25 to 35°N in latitude), and temporally over a two-week period from August 16th to August 31st, 2022, corresponding to the period of most intense rainfall. The standardized anomaly for observed rainfall is approximately 6 standard deviations above the climatological mean. It is evident that the ECMWF S2S model considerably underestimates rainfall intensity for forecasts initialized on July 21st, achieving only about one-third of the observed values. The ECMWF S2S forecasts gradually converge toward observations as the initialization dates approach the actual event. In contrast, FuXi-S2S exhibits superior forecast performance in predicting the intensity of extreme rainfall events earlier compared to ECMWF S2S. Specifically, FuXi-S2S predicts rainfall levels of at least 4 standard deviation above the climatological mean for forecasts initialized on July 21st, which is approximately 4 weeks in advance. Moreover, the spatial distributions of the standardized TP anomaly reveal that the FuXi-S2S predicted TP pattern more closely matches the observations.

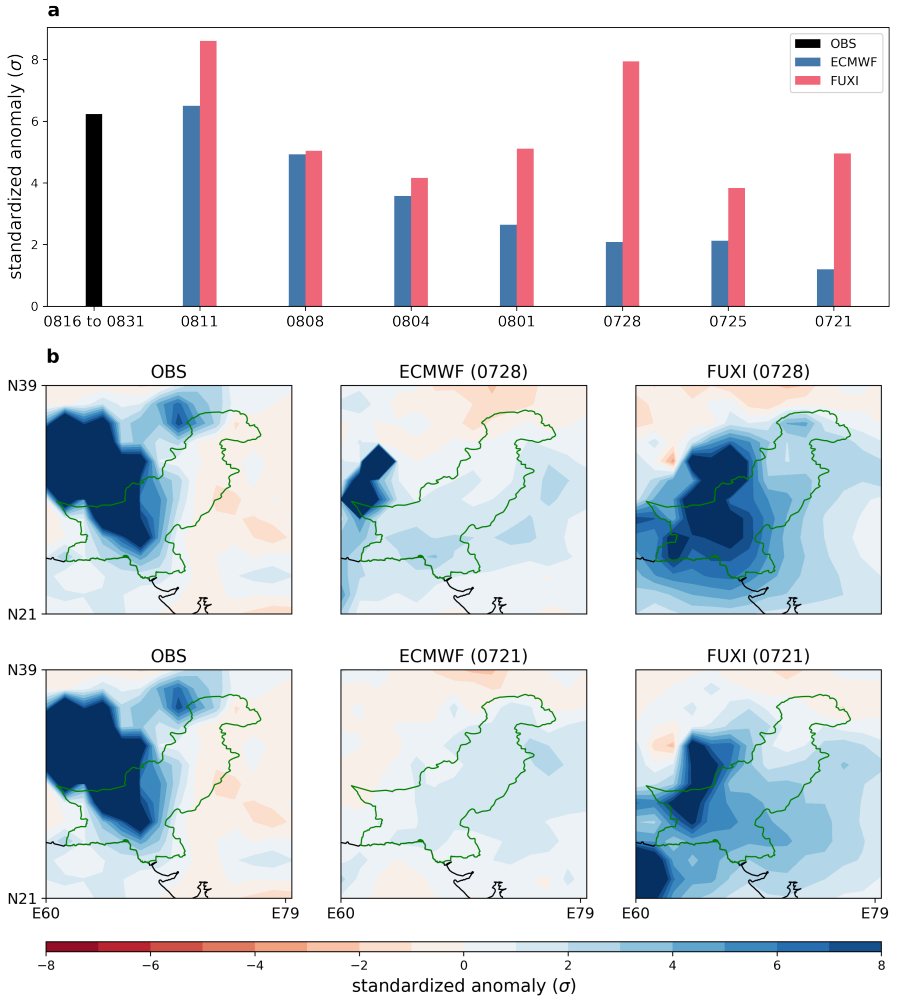


**Fig. 4:** Comparison of spatially and temporally averaged standardized TP anomaly (a) over the two weeks from August 16th to August 31st, 2022, showcasing GPCP observations (in black) alongside predictions from ECMWF S2S real-time forecasts (in blue) and FuXi-S2S forecasts (in red), with initialization dates: August 11th (0811), August 8th (0808), August 4th (0804), August 1st (0801), July 28th (0728), July 25th (0725), and July 21st (0721). For the comparison of temporally averaged standardized TP anomaly maps (b), the first column represents GPCP observations, while the second and third columns display predictions from ECMWF S2S and FuXi-S2S, respectively, with initialization dates on July 28th (0728, first row) and July 21st (0721, second row). Green contour indicates the boarder line of Pakistan.

### 3 Discussion

In this paper, we introduce FuXi-S2S, a machine learning based subseasonal forecasting model offering 42 days of global daily mean value forecasts at a daily temporal resolution and 1.5°spatial resolution. We compare FuXi-S2S with the ECMWF S2S reforecasts. Our analysis of the ensemble mean’s deterministic forecast skill shows that FuXi-S2S outperforms ECMWF S2S in predicting TP and OLR in terms of TCC, while also demonstrating comparable performance in predicting Z500 and T2M. Furthermore, FuXi-S2S demonstrates superior performance in forecasting TP, T2M, Z500 and OLR in terms of the ensemble forecast skill (RPSS), particularly over extra-tropics and land areas. FuXi-S2S also surpasses ECMWF S2S in extreme rainfall forecasts according to the globally-averaged BSS. Moreover, FuXi-S2S greatly enhances accuracy in predicting the MJO, extending skillful MJO prediction from 30 days to 36 days, which is a major source of subseasonal variability. In the context of the 2022 Pakistan floods, FuXi-S2S displays superior capability in predicting extreme rainfall earlier compared to ECMWF S2S.

Ensemble forecasting remains crucial, but computational constraints often limit the generation of subseasonal forecasts with sufficiently large ensemble sizes. Presently, the number of ensemble members across 11 forecast centers globally ranges from 4 to 51 [61]. However, recent research suggests that the optimal number of members for subseasonal forecasts could be significantly higher, potentially falling within the range of 100 to 200 members [62]. In our study, we generated and assessed a 51-member FuXi-S2S ensemble, constrained by memory limitations required for storing 20 years of data for evaluation. Despite these constraints, the FuXi-S2S model demonstrates potential in generating a larger member count at significantly lower computational costs.

The FuXi-S2S model exhibits the capacity to predict a diverse set of surface and upper-air variables, opening substantial opportunities for future exploration. This paper highlights its proficiency in predicting the MJO. We envision that FuXi-S2S could serve as a pivotal tool in investigating other primary modes of subseasonal variability, such as the Boreal Summer Intraseasonal Oscillation (BSISO), North Atlantic Oscillation (NAO), and East Asia-Pacific (EAP) pattern.

## 4 Methods

### 4.1 Data

ERA5 stands as the fifth iteration of the ECMWF reanalysis dataset, offering a rich array of surface and upper-air variables. It operates at a remarkable temporal resolution of 1 hour and a horizontal resolution of approximately 31 km, covering data from January 1950 to the present day [26]. Recognized for its expansive temporal and spatial coverage coupled with exceptional accuracy, ERA5 stands as the most comprehensive and precise reanalysis

archive globally. In our study, we utilize daily statistics derived from the 1-hourly ERA5 dataset, which maintains a spatial resolution of  $1.5^\circ$  ( $121 \times 240$  latitude-longitude grid points).

Alongside the ERA5 reanalysis data, a newly developed OLR dataset called the Climate Prediction Center (CPC) OLR (CBO) has emerged. Spanning from 1991 to the present day, this dataset undergoes near real-time updates. While showing slight differences in magnitude compared to the US National Oceanic and Atmospheric Administration (NOAA) Advanced Very High-Resolution Radiometer (AVHRR) OLR, the CBO dataset notably exhibits a high level of similarity in both pattern and magnitude of anomalies. In our work, we utilize the CBO data, possessing a spatial resolution of  $1^\circ$ , as the ground truth for OLR to identify MJO events. Furthermore, for the assessment of rainfall in the Pakistan region, observed rainfall data are sourced from the Global Precipitation Climatology Project (GPCP) dataset [63].

The FuXi-S2S model forecasts a total of 76 variables, encompassing 5 upper-air atmospheric variables across 13 pressure levels (50, 100, 150, 200, 250, 300, 400, 500, 600, 700, 850, 925, and 1000 hPa), and 11 surface variables. Among the upper-air atmospheric variables are geopotential (Z), temperature (T), u component of wind (U), v component of wind (V), and specific humidity (Q). The surface variables include 2-meter temperature (T2M), 2-meter dewpoint temperature (D2M), sea surface temperature (SST), outgoing long-wave radiation (OLR)<sup>1</sup>, 10-meter u wind component (U10), 10-meter v wind component (V10), 100-meter u wind component (U100), 100-meter v wind component (V100), mean sea-level pressure (MSL), total column water vapor (TCWV), and TP. Table 1 provides a comprehensive list of these variables along with their abbreviations.

The model’s training relies on 67 years of data spanning from 1950 to 2016, while evaluation involves a 5-year dataset from 2017 to 2021. Additionally, the dataset for the year 2022 undergoes evaluation and comparison against the ECMWF real-time S2S forecasts, specifically concerning the catastrophic flooding in Pakistan. More detailed evaluations of TP and MJO predictions for the year 2022 can be found in the supplementary material.

In certain cases, subseasonal forecasts receives regular updates through the implementation of the latest model, incorporating research discoveries tailored for operational use [64]. For instance, the ECMWF S2S reforecasts, often termed hindcasts, which are generated on-the-fly by employing the most recent model version available at the time of forecast generation. In our research, we utilize the ECMWF S2S reforecasts generated from model cycle C47r3. These reforecasts encompass initialization dates over 20 years, ranging from January 3, 2002, to December 29, 2021. The ECMWF S2S reforecasts are initialized twice weekly, aligning with the real-time forecasts. Additionally, our comparative analysis involves employing the 51-member ECMWF real-time S2S forecast for the year 2022. In the analysis encompassing testing data from 2017

---

<sup>1</sup>OLR, known as the negative of top net thermal radiation (TTR) in ECMWF convention.

**Table 1:** A summary of all the upper-air and surface variable names and their abbreviations in this paper.

Type	Full name	Abbreviation
upper-air variables	geopotential	Z
	temperature	T
	u component of wind	U
	v component of wind	V
	specific humidity	Q
surface variables	2-meter temperature	T2M
	2-meter dewpoint temperature	D2M
	sea surface temperature	SST
	outgoing longwave radiation	OLR
	top net thermal radiation	TTR
	10-meter u wind component	U10
	10-meter v wind component	V10
	100-meter u wind component	U100
	100-meter v wind component	V100
	mean sea-level pressure	MSL
	total column water vapor	TCWV
	total precipitation	TP

to 2021, anomalies for all variables are defined as deviations from the climatological mean calculated over the 15-year period from 2002 to 2016. Meanwhile, for the analysis based on testing data in the year 2022, the climatological mean is calculated over the period from 2002 to 2021.

To ensure equitable comparisons, we evaluate FuXi-S2S forecasts specifically on identical initialization dates corresponding to those utilized for both the ECMWF S2S reforecasts and forecasts. This approach facilitates a fair and direct assessment between FuXi-S2S and ECMWF S2S.

## 4.2 FuXi-S2S model

In the development of the FuXi-S2S model, we enhanced the FuXi base model by incorporating a perturbation module designed to introduce flow-dependent perturbations into the hidden features of the model. As depicted in Figure 5, the FuXi-S2S model consists of three primary components: a prior encoder, a posterior encoder (used for training only), and a latent decoder. The prior encoder processes weather parameters from two preceding time steps, denoted as  $\mathbf{X}^{t-1}$  and  $\mathbf{X}^t$ . It extracts the hidden feature  $\mathbf{h}^t$  (with dimensions of  $1536 \times 60 \times 120$ ) through 12 repeated transformer blocks. The input combines both upper-air and surface variables into a data cube with the dimensions of  $2 \times 76 \times 121 \times 240$ , representing two preceding time steps ( $t-1$  and  $t$ ), the number of input variables, and the latitude (H) and longitude (W) grid points, respectively. Furthermore, recognizing that the forecast error accumulates with increasing forecast lead time, we incorporate the forecast lead time ( $t$ ) as input to the encoder. Meanwhile, the encoder generates a low-rank multivariate Gaussian distribution (P), characterized by a mean vector  $\mu^t$  ( $128 \times 60 \times 120$ ), a covariance matrix  $\sigma^t$  ( $1536 \times 60 \times 120$ ), and a diagonal covariance matrix  $diag^t$  ( $128 \times 60 \times 120$ ).

The posterior encoder, used exclusively during the training phase and mirroring the prior encoder’s network structure, processes a data cube comprising both a preceding and the current time steps:  $\mathbf{X}^t$  and  $\mathbf{X}^{t+1}$ . Similar to the prior encoder, it predicts a low-rank multivariate Gaussian distribution (Q). Under the assumption of minimal atmospheric state changes between consecutive time steps  $t$  and  $t + 1$ , resulting in minor distribution variations, we calculate the Kullback-Leibler (KL) divergence loss ( $L_{KL}$ ) to quantify the difference between the distributions predicted by the prior (P) and posterior encoders (Q). This loss aims to maximize the similarity between the two distributions. During the training phase, intermediate perturbation vectors are sampled from the posterior distribution ( $z_q^t$ ), while during the testing phase, they are sampled from the prior distribution ( $z_p^t$ ). These vectors have dimensions of  $128 \times 60 \times 120$ . Depending on whether it is the training or testing phase, a learned mixture weight is applied to either  $z_q^t$  or  $z_p^t$  to derive the perturbation vector  $z^t$  ( $1536 \times 60 \times 120$ ). Subsequently, the latent decoder processes the perturbed hidden feature ( $\hat{h}^t = h^t + z^t$ ) through 24 repeated transform blocks and a fully connected layer, mapping it to the final output  $\hat{\mathbf{X}}^{t+1}$ . A L1 loss is applied between model output ( $\hat{\mathbf{X}}^{t+1}$ ) and the target  $\mathbf{X}^{t+1}$ . The overall loss function at each autoregressive step is thus determined by the following equation:

$$L = \lambda L_{KL}(P^t, Q^t) + |\hat{\mathbf{X}}^{t+1} - \mathbf{X}^{t+1}| \quad (1)$$

where  $\lambda$ , a tune-able coefficient balancing  $L_{KL}$  and L1, is set to  $1 \times 10^{-4}$  in this study. The design of this loss function serves two purposes: the first term ensures the perturbation vector closely approximates the true data distribution, while the second term ensures the prediction unaffected by any perturbation vectors  $z^t$ .

During the testing stage, as illustrated in Figure 5, the dashed line path is omitted, and the intermediate perturbation vector ( $z_p^t$ ) is sampled from the prior distribution P. Additionally, Perlin noise is introduced into the input data. For subseasonal ensemble forecasting, we employ 51 ensemble members. Each member incorporates 3 octaves of Perlin noise with a scaling factor of 0.5, and the number of periods of noise along each axis (channel, latitude, and longitude) is set to 1, 6 and 6, respectively. As illustrated in Supplementary Figure 10, the FuXi-S2S model, when enhanced with flow-dependent perturbations incorporated into its hidden features, demonstrates considerably improved forecast performance when compared to FuXi-S2S models that only utilize Perlin noise in the initial conditions or combine Perlin noise in the initial conditions with fixed perturbations added into the hidden features.

Similar to FuXi, an autoregressive, we utilize an autoregressive, multi-step loss function to mitigate cumulative errors over long lead times, as outlined in Lam et al. [21]. The training process follows an autoregressive training regime and a curriculum training schedule, incrementally increasing the number of autoregressive steps from 1 to 17. Each autoregressive step undergoes 1000 iterations of training. A batch size of 1 is used on each GPU. Optimization is

performed using the AdamW [65, 66] optimizer with the following parameters:  $\beta_1=0.9$  and  $\beta_2=0.95$ , an initial learning rate of  $2.5 \times 10^{-4}$ , and a weight decay coefficient of 0.1.

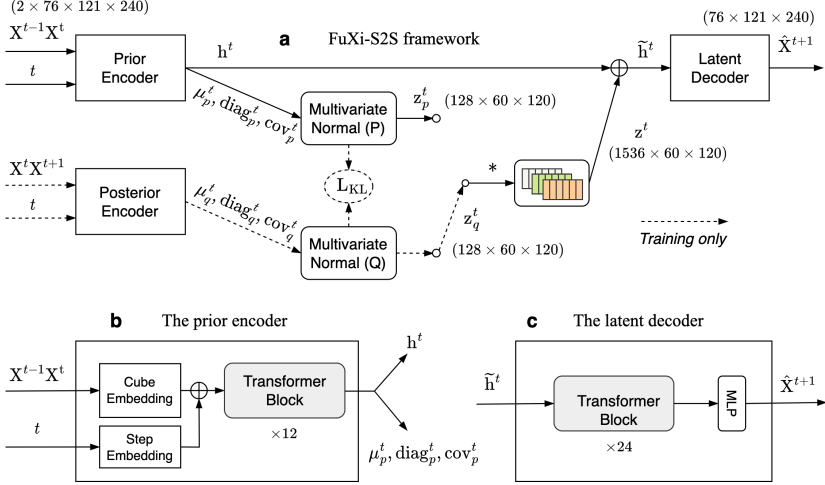


**Fig. 5:** Schematic diagram of the structures of the FuXi-S2S model.

### 4.3 Evaluation method

Prior to evaluation, each variable undergoes detrending process to eliminate the linear trend. This detrending step is essential for removing linear long-term trends that may be affected by external climate forcing. Subsequently, the deterministic forecast performance of the ensemble mean is evaluated using the latitude-weighted TCC, which is calculated as follows:

$$\text{TCC}(c, \tau, i, j) = \frac{\sum_{t_0 \in D} \hat{\mathbf{A}}_{c,i,j}^{t_0+\tau} \mathbf{A}_{c,i,j}^{t_0+\tau}}{\sqrt{\sum_{t_0 \in D} (\hat{\mathbf{A}}_{c,i,j}^{t_0+\tau})^2 \sum_{t_0 \in D} (\mathbf{A}_{c,i,j}^{t_0+\tau})^2}} \quad (2)$$

where  $t_0$  represents the forecast initialization time in the testing dataset  $D$ .  $H$ , and  $W$  denote the number of grid points in the latitude and longitude directions. The indices  $c$ ,  $i$ , and  $j$  correspond to variables, latitude and longitude coordinates, respectively.  $\tau$  refers to the forecast lead time steps added to  $t_0$ .  $\hat{\mathbf{A}}_{c,i,j}^{t_0+\tau}$  and  $\mathbf{A}_{c,i,j}^{t_0+\tau}$  are the differences between the forecast or observation and the climatological mean, with the climatological mean derived from data spanning the years from 2002 and 2016.

To evaluate the ensemble forecast performance, we use the RPSS [57, 58] which quantifies the comparison between the cumulative squared probability errors of a given forecast and a climatological forecast. The calculation of the RPSS metric necessitates prior determination of the ranked probability

scores (RPS) for both the forecast ( $\text{RPS}_{\text{forecast}}$ ) and the climatological forecast ( $\text{RPS}_{\text{clim}}$ ) should be calculated first. The RPS aggregates the squared probability errors across  $K$  ( $K = 3$  in this work) categories, such as tercile, arranged in ascending order. The tercile bounds are determined based on the average values over either one-week or two-week periods for each corresponding verification period. These calculations are performed separately for the forecast, observation (ERA5 data), and climatological forecast. The metric assesses the accuracy with which the probability forecast predicts the actual observation category. The RPS score is derived from the sum of the squared differences between the cumulative categorical forecast probability and its observed counterpart, where  $p_{O(i)} = 1$  denotes the observed category and  $p_{O(i)} = 0$  represents other categories:

$$\text{RPS}_{\text{forecast}} = \sum_{k=1}^K (F_{\text{forecast}(k)} - F_{O(k)}) \quad (3)$$

$$\text{RPS}_{\text{clim}} = \sum_{k=1}^K (F_{\text{clim}(k)} - F_{O(k)}) \quad (4)$$

where  $F_{\text{forecast}(k)} = \sum_{i=1}^k p_{\text{forecast}(i)}$ ,  $F_{\text{clim}(k)} = \sum_{i=1}^k p_{\text{clim}(i)}$ ,  $F_{O(k)} = \sum_{i=1}^k p_{O(i)}$  represent the  $k$ th components of the cumulative forecast, climatological, and observational distributions, respectively. And  $p_{\text{forecast}(i)}$ ,  $p_{\text{clim}(i)}$ ,  $p_{O(i)}$  correspond to the forecasted, climatological, and observed probability of the event's occurrence in category  $i$ . Crucially, the RPS is affected by both the forecast probabilities attributed to the observed category and the probabilities assigned to other categories. The RPS value varies between 0 and 1, where a lower value denotes a smaller forecast probability error, and thus a more accurate forecast. Specifically, a RPS value of 0 indicates a perfectly accurate categorical forecast. With the RPS values of both the forecast and the climatological forecast, the RPSS can be determined as:

$$\text{RPSS} = 1 - \frac{\langle \text{RPS}_{\text{forecast}} \rangle}{\langle \text{RPS}_{\text{clim}} \rangle} \quad (5)$$

where, the brackets  $\langle \dots \rangle$  denote the average of the  $\text{RPS}_{\text{forecast}}$  and  $\text{RPS}_{\text{clim}}$  values across all forecast–observation pairs. Since each forecast category is equally probable by design, the climatological forecast assumes a 33% probability of occurrence for each category. The RPSS metric serves a comparative measure against the climatological forecast. Its value range from  $-\infty$  to 1, where 1 corresponds to a perfect forecast and higher values suggest better forecast performance. A positive RPSS value indicates superior accuracy over the climatological forecast, while a negative value suggests inferior accuracy. A value of zero suggests that the forecast has no added skill compared to the climatological forecast.

Additionally, we use the BSS[58] to evaluate the performance of extreme forecasts. The BSS, a widely used metric for assessing the quality of categorical

probabilistic forecasts, can be considered as a special case of the RPSS with two forecast categories [67]. The BSS is computed using the following equation:

$$\text{BSS} = 1 - \frac{\langle \text{BS}_{\text{forecast}} \rangle}{\langle \text{BS}_{\text{clim}} \rangle} \quad (6)$$

where  $\text{BS}_{\text{forecast}}$  and  $\text{BS}_{\text{clim}}$  represent the Brier Scores (BS) [68] for the model's forecast and the climatological forecast, respectively. Similar to the RPS, the BS quantifies the mean squared difference between the predicted probabilities and observations (either 0 or 1) in binary probabilistic forecasts. In this study, the BSS is calculated for the ensemble mean of both FuXi-S2S and ECMWF S2S, using the 90th climatological percentiles as the threshold for extreme events. The BS ranges from 0 to 1, with lower values indicating a better agreement between ensemble forecasts and observations with 0 suggesting the best possible BS score. On the contrary, a higher BSS, up to a maximum of 1, indicates better performance. The BSS measures the improvement of a forecast's BS ( $\text{BS}_{\text{forecast}}$ ) relative to that of a climatological forecast ( $\text{BS}_{\text{clim}}$ ) as reference. A BSS of one indicates a perfect forecast, zero denotes no improvement over climatology, and negative values suggest inferior performance compared to climatology.

The evolution of MJO is typically characterized using the Real-time Multivariate MJO (RMM) index, as originally developed by Wheeler and Hendon [50]. The RMM1 and RMM2 indices represent the first and second principal components of the combined Empirical Orthogonal Function (EOF). This EOF is derived based on the daily mean values of OLR, zonal wind at 850 hPa (U850), and zonal wind at 200 hPa (U200), all averaged within the latitude range of 15°N and 15°S [69]. In this study, we use the EOFs derived by Wheeler and Hendon (2004) [50]. To obtain the predicted MJO indices, the data from both FuXi-S2S and ECMWF S2S are firstly interpolated from a spatial resolution of 1.5° to a 2.5°. The amplitude and phase of the MJO are respectively defined by the formulas:  $\sqrt{\text{RMM1}^2(t) + \text{RMM2}^2(t)}$  and  $\tan^{-1} \frac{\text{RMM2}^2(t)}{\text{RMM1}^2(t)}$ . To assess the quality of the MJO forecasts, we calculate the bivariate COR using the following equation:

$$\text{COR}(\tau) = \frac{\sum_{t=1}^N [a_1(t)b_1(t, \tau) + a_2(t)b_2(t, \tau)]}{\sqrt{\sum_{t=1}^N [a_1^2(t) + a_2^2(t)]} \sqrt{\sum_{t=1}^N [b_1^2(t, \tau) + b_2^2(t, \tau)}} \quad (7)$$

where  $a_1(t)$  and  $a_2(t)$  are the observed RMM1 and RMM2 at time  $t$  derived from the ERA5 reanalysis dataset. Correspondingly,  $b_1(t, \tau)$  and  $b_2(t, \tau)$  represent the forecasts for time  $t$  with a lead time of  $\tau$  days, respectively.  $N$  denotes the number of total predictions. We apply the threshold of  $\text{COR} = 0.5$  for skillful prediction [69].

## Data Availability Statement

We downloaded a subset of the daily statistics from the ERA5 hourly data from the official website of Copernicus Climate Data (CDS) at <https://cds.climate.copernicus.eu/cdsapp#!/software/app-c3s-daily-era5-statistics>. The ECMWF S2S data were obtained from <https://apps.ecmwf.int/datasets/data/s2s/>. The 1°CPC OLR data are provided by the NOAA PSL from their website of <https://psl.noaa.gov>. Rainfall data from the Global Precipitation Climatology Project (GPCP) was obtained from the National Oceanic and Atmospheric Administration (NOAA), specifically the National Centers for Environmental Information (NCEI), which is accessible at <https://www.ncei.noaa.gov/products/global-precipitation-climatology-project>.

## Code Availability Statement

Calculation of MJO index is based on the EOFs derived by Wheeler and Hendon (2004) [50] that are available at <https://doi.org/10.5281/zenodo.5806377> [70].

The implementation of Perlin noise is based on publicly available from the GitHub repository: <https://github.com/pvigier/perlin-numpy>.

## Acknowledgements

This work was supported by the National Key R&D Program of China under Grant 2021YFA0718000 and National Natural Science Foundation of China, Grant 42175052. We extend our sincere gratitude to the researchers at ECMWF for their invaluable contributions to the collection, archival, dissemination, and maintenance of the ERA5 reanalysis dataset and ECMWF S2S reforecast and real-time forecast data. .

## Competing interests

The authors declare no competing interests.

## References

- [1] National Academies of Sciences, E.: Next Generation Earth System Prediction: Strategies for Subseasonal to Seasonal Forecasts. National Academies Press, Washington, DC (2016)
- [2] White, C.J., *et al.*: Potential applications of subseasonal-to-seasonal (s2s) predictions. *Meteorological Applications* **24**(3), 315–325 (2017)
- [3] Pegion, K., *et al.*: The subseasonal experiment (subx): A multimodel sub-seasonal prediction experiment. *Bulletin of the American Meteorological Society* **100**(10), 2043–2060 (2019)

- [4] White, C.J., *et al.*: Advances in the application and utility of subseasonal-to-seasonal predictions. *Bulletin of the American Meteorological Society* **103**(6), 1448–1472 (2022)
- [5] Domeisen, D.I., *et al.*: Advances in the subseasonal prediction of extreme events: relevant case studies across the globe. *Bulletin of the American Meteorological Society* **103**(6), 1473–1501 (2022)
- [6] Merryfield, W.J., *et al.*: Current and emerging developments in sub-seasonal to decadal prediction. *Bulletin of the American Meteorological Society* **101**(6), 869–896 (2020)
- [7] Mouatadid, S., *et al.*: Adaptive bias correction for improved subseasonal forecasting. *Nature Communications* **14**(1), 3482 (2023)
- [8] Vitart, F., Robertson, A.W., Anderson, D.L.: Subseasonal to seasonal prediction project: Bridging the gap between weather and climate. *Bulletin of the World Meteorological Organization* **61**(2), 23 (2012)
- [9] Vitart, F., *et al.*: Sub-seasonal predictions. ECMWF Tech. Memo. **738** (2014)
- [10] Lorenz, E.N.: Deterministic Nonperiodic Flow. *J. Atmos. Sci.* **20**(2), 130–148 (1963)
- [11] Weyn, J.A., Durran, D.R., Caruana, R., Cresswell-Clay, N.: Sub-seasonal forecasting with a large ensemble of deep-learning weather prediction models. *Journal of Advances in Modeling Earth Systems* **13**(7), 2021–002502 (2021)
- [12] Vitart, F.: Evolution of ecmwf sub-seasonal forecast skill scores. *Quarterly Journal of the Royal Meteorological Society* **140**(683), 1889–1899 (2014)
- [13] Saha, S., *et al.*: The ncep climate forecast system version 2. *Journal of climate* **27**(6), 2185–2208 (2014)
- [14] Monhart, S., *et al.*: Skill of subseasonal forecasts in europe: Effect of bias correction and downscaling using surface observations. *Journal of Geophysical Research: Atmospheres* **123**(15), 7999–8016 (2018)
- [15] Domeisen, D.I., White, C.J., Afargan-Gerstman, H., Muñoz, Á.G., Janiga, M.A., Vitart, F., Wulff, C.O., Antoine, S., Ardilouze, C., Batté, L., *et al.*: Advances in the subseasonal prediction of extreme events: relevant case studies across the globe. *Bulletin of the American Meteorological Society* **103**(6), 1473–1501 (2022)
- [16] Nowak, K., Webb, R., Cifelli, R., Brekke, L.: Sub-seasonal climate forecast

- rodeo. In: 2017 AGU Fall Meeting, New Orleans, LA, pp. 11–15 (2017)
- [17] Vitart, F., *et al.*: Outcomes of the wmo prize challenge to improve subseasonal to seasonal predictions using artificial intelligence. *Bulletin of the American Meteorological Society* **103**(12), 2878–2886 (2022)
- [18] Cohen, J., *et al.*: S2s reboot: An argument for greater inclusion of machine learning in subseasonal to seasonal forecasts. *Wiley Interdisciplinary Reviews: Climate Change* **10**(2), 00567 (2019)
- [19] Richardson, D.S.: Measures of skill and value of ensemble prediction systems, their interrelationship and the effect of ensemble size. *Quarterly Journal of the Royal Meteorological Society* **127**(577), 2473–2489 (2001)
- [20] Pathak, J., *et al.*: Fourcastnet: A global data-driven high-resolution weather model using adaptive fourier neural operators. Preprint at <https://arxiv.org/abs/2202.11214> (2022)
- [21] Lam, R., *et al.*: Learning skillful medium-range global weather forecasting. *Science* (2023)
- [22] Bi, K., *et al.*: Accurate medium-range global weather forecasting with 3d neural networks. *Nature* (2023)
- [23] Chen, L., *et al.*: Fuxi: A cascade machine learning forecasting system for 15-day global weather forecast. *npj Climate and Atmospheric Science*, 1–11 (2023)
- [24] Zhong, X., Chen, L., , Liu, J., Liu, C., Qi, Y., Li, H.: FuXi-Extreme: Improving extreme rainfall and wind forecasts with diffusion model (2023)
- [25] Haiden, T., *et al.*: Evaluation of ECMWF forecasts, including the 2021 upgrade (2021)
- [26] Hersbach, H., *et al.*: The era5 global reanalysis. *Q. J. R. Meteorol. Soc.* **146**(730), 1999–2049 (2020)
- [27] He, S., Li, X., DelSole, T., Ravikumar, P., Banerjee, A.: Sub-seasonal climate forecasting via machine learning: Challenges, analysis, and advances. *Proceedings of the AAAI Conference on Artificial Intelligence* **35**(1), 169–177 (2021)
- [28] Friedman, J.H.: Greedy function approximation: a gradient boosting machine. *Annals of statistics*, 1189–1232 (2001)
- [29] Chen, T., Guestrin, C.: Xgboost: A scalable tree boosting system. In: *Proceedings of the 22nd Acm Sigkdd International Conference on Knowledge*

- Discovery and Data Mining, pp. 785–794 (2016)
- [30] Tibshirani, R.: Regression shrinkage and selection via the lasso. *Journal of the Royal Statistical Society Series B: Statistical Methodology* **58**(1), 267–288 (1996)
  - [31] Jalali, A., Ravikumar, P., Sanghavi, S.: A dirty model for multiple sparse regression. *IEEE Transactions on Information Theory* **59**(12), 7947–7968 (2013)
  - [32] Sutskever, I., Vinyals, O., Le, Q.V.: Sequence to sequence learning with neural networks. *Advances in neural information processing systems* **27**, 3104–3112 (2014)
  - [33] Kiefer, S.M., Lerch, S., Ludwig, P., Pinto, J.G.: Can machine learning models be a suitable tool for predicting central european cold winter weather on subseasonal to seasonal time scales? *Artificial Intelligence for the Earth Systems* **2**(4), 1–16 (2023)
  - [34] Breiman, L.: Random forests. *Machine learning* **45**, 5–32 (2001)
  - [35] de Andrade, F.M., Coelho, C.A., Cavalcanti, I.F.: Global precipitation hindcast quality assessment of the subseasonal to seasonal (s2s) prediction project models. *Climate Dynamics* **52**(9-10), 5451–5475 (2019)
  - [36] Molteni, F., Buizza, R., Palmer, T.N., Petroliagis, T.: The ecmwf ensemble prediction system: Methodology and validation. *Quarterly Journal of the Royal Meteorological Society* **122**(529), 73–119 (1996)
  - [37] Madden, R.A., Julian, P.R.: Detection of a 40–50 day oscillation in the zonal wind in the tropical pacific. *Journal of Atmospheric Sciences* **28**(5), 702–708 (1971)
  - [38] Madden, R.A., Julian, P.R.: Description of global-scale circulation cells in the tropics with a 40–50 day period. *Journal of Atmospheric Sciences* **29**(6), 1109–1123 (1972)
  - [39] Zhang, C.: Madden-julian oscillation. *Reviews of Geophysics* **43**(2) (2005)
  - [40] Zhang, C.: Madden-julian oscillation: Bridging weather and climate. *Bulletin of the American Meteorological Society* **94**(12), 1849–1870 (2013)
  - [41] Zhang, C., *et al.*: Cracking the mjo nut. *Geophysical Research Letters* **40**(6), 1223–1230 (2013)
  - [42] Neena, J., *et al.*: Predictability of the madden–julian oscillation in the intraseasonal variability hindcast experiment (isvhe). *Journal of Climate* **27**(12), 4531–4543 (2014)

- [43] Kim, H., Vitart, F., Waliser, D.E.: Prediction of the madden–julian oscillation: A review. *Journal of Climate* **31**(23), 9425–9443 (2018)
- [44] Jiang, X., *et al.*: Fifty years of research on the madden-julian oscillation: Recent progress, challenges, and perspectives. *Journal of Geophysical Research: Atmospheres* **125**(17), 2019–030911 (2020)
- [45] Silini, R., *et al.*: Improving the prediction of the madden–julian oscillation of the ecmwf model by post-processing. *Earth System Dynamics* **13**(3), 1157–1165 (2022)
- [46] Kim, H., Ham, Y.G., Joo, Y.S., Son, S.W.: Deep learning for bias correction of mjo prediction. *Nature Communications* **12**(1)
- [47] Silini, R., Barreiro, M., Masoller, C.: Machine learning prediction of the madden-julian oscillation. *npj Climate and Atmospheric Science* **4**(1), 57 (2021)
- [48] Toms, B.A., Kashinath, K., Yang, D., *et al.*: Testing the reliability of interpretable neural networks in geoscience using the madden–julian oscillation. *Geoscientific Model Development* **14**(7), 4495–4508 (2021)
- [49] Delaunay, A., Christensen, H.M.: Interpretable deep learning for probabilistic mjo prediction. *Geophysical Research Letters* **49**(16), 2022–098566 (2022)
- [50] Wheeler, M.C., Hendon, H.H.: An all-season real-time multivariate mjo index: Development of an index for monitoring and prediction. *Monthly weather review* **132**(8), 1917–1932 (2004)
- [51] Lim, Y., Son, S.-W., Kim, D.: Mjo prediction skill of the subseasonal-to-seasonal prediction models. *Journal of Climate* **31**(10), 4075–4094 (2018)
- [52] Zhu, B., Wang, B.: The 30-60-day convection seesaw between the tropical indian and western pacific oceans. *Journal of the Atmospheric Sciences* **50**, 184–199 (1993)
- [53] Walker, G.T.: Correlations in seasonal variations of weather. viii, a further study of world weather. *Men. Indian Meteor. Dept.* **24**, 275–332 (1924)
- [54] Huang, R.H.: Influence of the heat source anomaly over the western tropical pacific for the subtropical high over east asia. In: *International Conference on the General Circulation of East Asia*. Chendu, China, April 10-15, 1987, pp. 40–50 (1987)
- [55] Huang, R., Li, W.: Influence of heat source anomaly over the western tropical pacific on the subtropical high over east asia and its physical

- mechanism. *Chin. J. Atmos. Sci* **12**(s1), 107–116 (1988)
- [56] Nitta, T.: Convective activities in the tropical western pacific and their impact on the northern hemisphere summer circulation. *Journal of the Meteorological Society of Japan. Ser. II* **65**(3), 373–390 (1987)
- [57] Epstein, E.S.: A scoring system for probability forecasts of ranked categories. *Journal of Applied Meteorology (1962-1982)* **8**(6), 985–987 (1969)
- [58] Wilks, D.S.: *Statistical Methods in the Atmospheric Sciences* vol. 100, 3rd edn. (2011)
- [59] Hong, C.-C., Huang, A.-Y., Hsu, H.-H., Tseng, W.-L., Lu, M.-M., Chang, C.-C.: Causes of 2022 pakistan flooding and its linkage with china and europe heatwaves. *npj Climate and Atmospheric Science* **6**(1), 163 (2023)
- [60] Dunstone, N., Smith, D.M., Hardiman, S.C., Davies, P., Ineson, S., Jain, S., Kent, C., Martin, G., Scaife, A.A.: Windows of opportunity for predicting seasonal climate extremes highlighted by the pakistan floods of 2022. *Nature Communications* **14**(1), 6544 (2023)
- [61] Vitart, F., *et al.*: The subseasonal to seasonal (s2s) prediction project database. *Bulletin of the American Meteorological Society* **98**(1), 163–173 (2017)
- [62] Buizza, R.: Introduction to the special issue on “25 years of ensemble forecasting”. *Quarterly Journal of the Royal Meteorological Society* **145**(S1), 1–11 (2019)
- [63] Adler, R.F., Sapiano, M.R., Huffman, G.J., Wang, J.-J., Gu, G., Bolvin, D., Chiu, L., Schneider, U., Becker, A., Nelkin, E., *et al.*: The global precipitation climatology project (gpcp) monthly analysis (new version 2.3) and a review of 2017 global precipitation. *Atmosphere* **9**(4), 138 (2018)
- [64] Stan, C., *et al.*: Advances in the prediction of mjo teleconnections in the s2s forecast systems. *Bulletin of the American Meteorological Society* **103**(6), 1426–1447 (2022)
- [65] Kingma, D.P., Ba, J.: Adam: A Method for Stochastic Optimization. Preprint at <https://arxiv.org/abs/1412.6980> (2017)
- [66] Loshchilov, I., Hutter, F.: Decoupled weight decay regularization. In: *International Conference on Learning Representations* (2017)
- [67] Weigel, A.P., Liniger, M.A., Appenzeller, C.: The discrete brier and ranked probability skill scores. *Monthly Weather Review* **135**(1), 118–124

(2007)

- [68] Brier, G.W.: Verification of Forecasts Expressed in Terms of Probability. *Monthly Weather Review* **78**(1), 1 (1950)
- [69] Rashid, H.A., Hendon, H.H., Wheeler, M.C., Alves, O.: Prediction of the madden–julian oscillation with the poama dynamical prediction system. *Climate Dynamics* **36**, 649–661 (2011)
- [70] Wang, S.: A Multivariate Index for Tropical intraseasonal Oscillations based on the Seasonally-varying Modal Structures. Zenodo (2021). <https://doi.org/10.5281/zenodo.5806377>. <https://doi.org/10.5281/zenodo.5806377>